CLM-R288

CLM-R288

Flow simulations for a glow discharge laser

W. Arter
D. F. Fletcher
A. C. Selden

UK ATOMIC ENERGY AUTHORITY

Culham Laboratory

CLM-R288

Flow simulations for a glow discharge laser

W. Arter, D. F. Fletcher, A. C. Selden
Culham Laboratory, Abingdon, Oxon OX14 3DB

Abstract

We describe the results of numerical calculations performed in order to improve understanding of the flow in a glow discharge laser. The Harwell-FLOW3D code was used to model 2-D incompressible flow past a triangular obstacle (representing a design of laser cathode) in a duct. Substantial numerical difficulties were encountered due to the flow being in the laminar/turbulent transition regime, but these were largely overcome. A series of time-dependent calculations including a model heat equation, demonstrate the effect of varying inlet speed on the region downstream of the obstacle.

Culham Laboratory
United Kingdom Atomic Energy Authority
Abingdon
Oxfordshire OX14 3DB

November 1988

ISBN: 085311 1723
£8.00

Contents

1. Introduction

At Culham Laboratory a considerable amount of work has been carried out to improve the performance of multi-kW glow discharge lasers [1]. This paper is concerned with one aspect of this work, namely the simulation of the gas flow behaviour in the region of the discharge. The availability of both user-friendly computational fluid dynamics (CFD) codes and modern super-computers (such as the CRAY-2) means that it is now possible to study fluid flow in regimes and geometries which were unthinkable less than ten years ago.

In this paper we are concerned with an apparently simple problem, namely the study of the gas flow past the cathode in a 2-D Cartesian duct configuration. We have chosen to use the Harwell code FLOW3D [2,3] in this work since it is readily available and we are familiar with its use. FLOW3D allows the user to solve coupled fluid flow and heat transfer problems in complex geometries using body-fitted coordinates. It can be used to model steady or unsteady, compressible or incompressible flow. The flow may be laminar or turbulent.

The aim of this work is to improve our understanding of flow conditions in the region of the cathode and use this knowledge to enhance the overall performance of the system. In this paper we describe the results obtained in the first stage of the study. The calculations reported upon here were carried out in order to demonstrate the capability of modern CFD codes and to obtain some qualitative results to compare with observations.

The paper is organised as follows: in Section 2 we describe the problem and the important fluid dynamic parameters associated with it. In Section 3 we describe the numerical difficulties encountered in performing accurate simulations. In Section 4 we concentrate on understanding the physics of the problem. Finally, we present some conclusions and suggestions for future work in Section 5.

2. Description of the Problem

In this section we give a description of the flow geometry and the associated fluid flow parameters. In this work we are concerned with modelling the gas flow in the region of the cathode. This is located in a duct which is approximately 500 mm long in the flow (x) direction and 60 mm wide in y. We have simplified the problem by considering a 2-D geometry, which is justified provided that we are not concerned with modelling edge effects. Figure 1 shows a schematic representation of the flow geometry. This consists of a 2-D channel with a bluff body (the cathode) located towards one side of the channel. The standard cathode is triangular in shape, with the (rounded) apex facing upstream: we hope to use other geometrical configurations in later work.

In the actual laser the working fluid is a mixture of He, N_2 and CO_2 (in the ratio 3:2:1) at a reduced pressure of 50 mb or 5 kPa (the reference pressure) and at an inlet temperature of 20°C. In the present simulations we used the thermophysical properties of air as these are similar to those of the real gas. At this temperature and pressure the gas has a density of 0.026 kg/m^3 and a dynamic viscosity of 2.5×10^{-5} kg/m/s [4]: we assume a Prandtl number (ratio of viscous to thermal diffusivity) of 0.7. The flow velocity is approximately uniform across the channel with a typical value of the order of u_0 = 50 m/s. This gives a channel Reynolds number of

$$Re_{chan} = 1560. \tag{1}$$

The Reynolds number based on a characteristic dimension d of the obstacle (assumed to be 9 mm) is given by

$$Re = 470. \tag{2}$$

The results from a variety of experimental studies of flow past a cylinder are presented in Reference 5. These show that the flow starts to become unsteady for Reynolds numbers above about 40. For Reynolds numbers below this value there is a stationary recirculation zone behind the cylinder. Above this Re vortices are shed periodically from each side of the cylinder: the Strouhal number

$$S = fd/u_0 \tag{3}$$

is the dimensionless measure of the shedding frequency f. The second plate in Reference 5 shows a symmetrical von Karman vortex street behind a cylinder for Re = 300. At this value the vortex street is beginning to show signs of instability. Figure 2 shows the dependence of the flow regime on the Reynolds number schematically. Thus in our application we would expect to get a vortex street downstream of the cylinder. Photographs of a vortex street are shown in Figure 3. Most previous computational studies of this phenomenon (e.g. Reference 6) are concerned with cylinders in an extended or infinite flow domain. These types of calculations require the use of very accurate solution methods as will be discussed in the next section.

Treating the gas mixture as an ideal gas (with the ratio of the specific heats taking a value of 1.4) gives an approximate sound speed of 510 m/s. Thus the Mach number is approximately 0.1 and the flow can be treated as incompressible in the absence of significant heating. Nevertheless, the heating of the gas by the glow discharge is sufficiently strong that a fully compressible treatment is needed. Unfortunately, we were not able to obtain converged results for compressible flow (see Section 3): the only reliable calculations described here use a model heat equation

$$\frac{\partial T}{\partial t} = -u\frac{\partial T}{\partial x} - v\frac{\partial T}{\partial y} + \kappa\nabla^2 T + S(x,y). \tag{4}$$

In (4), the terms on the right represent respectively the advection of temperature T, its diffusion at a rate with coefficient $\kappa = 1.37 \times 10^{-3}$ m^2/s and a heat source

$$S(x,y) = M \begin{cases} \text{constant} & r < a \\ \exp(-[r-a]^2/\delta^2) & a < r < a + \frac{5}{2}\delta \\ 0 & \text{otherwise} \end{cases} \tag{5}$$

where $r^2 = (x - x_s)^2 + (y - y_s)^2$. $S(x,y)$ represents a uniform heat source in a circular region of radius a centred on the point (x_s, y_s) that tapers off to zero in a surrounding annulus of width $\frac{5}{2}\delta$. a = 20 mm and (x_s, y_s) = (52, 25)mm, so the heat source is downstream and below the

obstacle as drawn in Figure 1. $\delta = 2$ mm and the normalisation constant M ensures a given total power input of 27 kW/m.

The other equations employed are standard for modelling incompressible flow. The thermal boundary conditions are that the inlet fluid and the cathode are isothermal at $T = 20°C$ and that the duct walls are adiabatic. For the flow, developed boundary conditions are specified at the outlet,

viz.

$$v = 0, \qquad \frac{\partial u}{\partial x} = 0, \tag{6}$$

and the inlet velocity profile is tapered near the walls, but otherwise uniform. Elsewhere, no-slip conditions are enforced.

3. Numerical Analytic Aspects of the Problem.

3.1 Coarse meshes

The work was begun in the hope that simulations using relatively coarse meshing, particularly in space, could produce reasonable results accurate to say within 10-20%. Upwind schemes such as are implemented in Harwell-FLOW3D can provide such accuracy for some flows, especially if only gross features are required. This motivated the use of meshes with $N_y = 30$ cells across the duct and a proportionate number along it. Although the grid was body fitted and thus non-uniform, no attempt was made to cluster cells where boundary layers might be expected.

Using the default options of FLOW3D, it proved possible to iterate out a steady solution. However, the same iteration repeated on a grid with $N_y = 60$ failed to converge, suggesting that the steady-state coarse mesh result was spurious. A natural interpretation is in terms of an excess of numerical viscosity: the hybrid differencing scheme employed for the dominant advective terms is such that truncation errors are always viscous in nature. The errors on the coarse mesh are sufficiently large that the effective Reynolds number is small enough for a steady numerical

solution to exist, much as it does in reality for $Re < 40$.

Time-dependent calculations were begun on the $N_y = 60$ grid, using the SIMPLE algorithm (the PISO algorithm proved to be unstable) with backward time differencing. The two numerical parameters remaining at our disposal are the time step Δt and the maximum amount ϵ_M by which mass conservation can be violated [2]. Two otherwise identical runs, but with Δt smaller by a factor 10 in the second, gave results differing by nearly a factor of two in such gross quantities as the shedding frequency and the maximum temperature reached.

In the hope that compressibility might help convergence (and because it is the more physically relevant case), much effort was devoted to the compressible problem. It is necessary to specify the pressure at the outlet: $p = p_{ref}$ (the reference pressure) was enforced. About a dozen different values of $(\Delta t, \epsilon_M)$ were tried - decreasing Δt and ϵ_M tended to favour steady solutions. Time dependence was found at other parameters, apparently because the error in the unconverged iterations acts as a forcing [7]. The steady state solutions gave a maximum temperature T_{max} as much as twice that of the time dependent ones. Clearly little reliance can be placed on any of these results.

3.2 Producing a sufficiently fine mesh

We are led to attempt direct simulation of the problem, namely to attempt to resolve every significant feature of (at least) the flow and pressure fields. To this end, the tapering, or smoothing of the heat source and inlet velocity field was added. The boundary layer surrounding the cathode is likely to be of crucial importance. No estimate for its thickness δ, even in the case of a circular obstacle appear to be available [8]. For a flow impinging on a flat plate $x = 0$ of form $u = -kx$ at large distance

$$\delta_{FP} = 0.65(\nu/k)^{1/2} \qquad (7)$$

whereas for flow past a thin aerofoil

$$\delta_{TA} = 1.74\left(\frac{\nu x}{u}\right)^{1/2} \qquad (8)$$

Taking plausible values for $k = 50$ m/s/0.03 m, $x = d = 0.009$ m, $u = 50$ m/s, gives $\delta_{FP} = 0.5$ mm and $\delta_{TA} = 0.7$ mm. Note that $d/\sqrt{Re} = 0.4$ mm. Assuming a minimum of three points is needed to resolve a layer, these estimates imply we should take Δx, the mesh-spacing, no larger than 0.2 mm. An approximately uniform grid of this size involves 2×10^5 cells: results from the coarser meshes indicate the likely computation time will be prohibitive, even on a CRAY-2.

Fortunately, by judicious use of constraint lines it is possible to use the Harwell supplied grid generation package to cluster points around the cathode. However, this exercise is far from trivial as the constraint lines must 'bend' toward the cathode, hence the mesh can become unacceptably distorted unless care is taken. Choosing the cathode so that it is relatively shorter along the flow direction helps somewhat. The interface to the package is also very long-winded and it proved necessary to write a code to generate input for it. Figure 4 shows the final choice of constraint lines.

The selected grid has $N_y = 106$ ($N_x = 178$): far from the cathode the typical spacing is 1 mm - no effort has been made to cluster cells near the duct walls. It is hoped that tapering the inlet profile has a favourable effect on the width of the wall layers. Further, considered purely as a 2-D channel flow, no time dependence is to be expected below $Re_{chan} = 3000$ [9]. The above spacings are close to the finest that yield a grid that can be manipulated interactively. (Four copies of a three-component (x,y,z) mesh have to be generated because, even though our problem is 2-D, FLOW3D is an intrinsically 3-D code.)

3.3 The fine mesh

We make the temporal mesh fine, too. Based on the data of Reference 10 for a circular obstacle, we would expect a shedding frequency of 1 kHz - we choose $\Delta t = 5/3 \times 10^{-5}$ s, giving 60 timesteps per period. The remaining freedoms at our disposal are firstly the initial conditions, for which we take $T = 20°C$ everywhere, and downstream of the cathode we

perturb the flow field at the 10% level by a von Karman vortex street, viz.,

$$u(x,y) + iv(x,y) = 50 +$$

$$\frac{c}{2a}\left(\frac{1}{1+\exp(-i\pi[z-z_c-ib]/a)} - \frac{1}{1-\exp(-i\pi[z-z_c+ib]/a)}\right), \qquad (9)$$

where $i^2 = -1$, $z = x + iy$ and the parameters $a = 0.022$, $b = 0.005$, $z_c = 0.04975$, $c = 0.186$ are selected on the basis of previous experience.

It is natural to use the FLOW3D default differencing, namely hybrid in space and backward in time. This is in line with the recommendations of Ciofalo [11], who treats the transient flow past a backward-facing step. Strictly, Ciofalo uses centred space differencing, but then our model heat equation diverges. He recommends use of the tolerance $\epsilon_M/\dot{M} = 5 \times 10^{-4}$ where $\dot{M}$ is the total mass flow, but we are less restrictive, as taking $\epsilon_M = 10^{-6}$ kg/mm/s gives $\epsilon_M/\dot{M} = 0.013$. The first run, of 600 timesteps (the velocity field was inadvertently reinitialised after 200 steps), is important because the final fields were used as the standard initial conditions for subsequent runs (summarised in Table 1).

The table shows that doubling the timestep or reducing ϵ_M to 10^{-7} leads to unacceptable changes in the shedding frequency, although the maximum temperature might be said to be converged. Observe that it is not cost-effective to double Δt, as N_{it}, the number of iterations per timestep, trebles: $N_{it}/\Delta t$ is an accurate measure of the cost of a run. (The computer time consumed per iteration increases only slightly when the higher order schemes are used.)

Two other spatial differencing schemes are available in FLOW3D for the dominant advective terms: HUW which is 2nd order accurate and QUICK which is 3rd order. The increase in formal accuracy does seem to result in better results, in that the calculated f are less discrepant, but even for QUICK, f changes by 10% as ϵ_M is reduced from 10^{-6} to 10^{-7}. Note that in all cases, less accuracy implies a smaller flow (as measured by min and max $|v|$) and a lower shedding frequency, consistent with the idea that "errors = extra viscosity". The frequency for the

first entry in the table is perhaps the most anomalous: however we were able to verify that it did not depend on initial conditions by restarting the run with the fields generated by the same scheme and Δt, but with $\epsilon_M = 10^{-7}$ (third entry in the table).

The most reliable results, showing only few per cent changes in f and the extrema of the fields as ϵ_M and Δt vary, are obtained using QUICK combined with Crank-Nicolson time differencing, which is 2nd order accurate in time. Observe that the higher order accuracy costs very little more. These runs will be discussed more fully in the next section.

We now try to understand why Ciofalo [11] should prefer not to use the QUICK/Crank-Nicolson option. Certainly, QUICK takes three times more iterations than hybrid differencing. Our experience suggests that the pressure field just downstream of the cathode is prone to spurious Δt-scale oscillations (see Figure 5), although these can be virtually eliminated by reducing ϵ_M to 10^{-7}, and in any case they appear to have no significant dynamical effects. Further, sudden changes in the inlet speed (imposed in the study in the next section) lead to similar, but much larger amplitude oscillations. Thus our only reason for preferring QUICK is its greater accuracy, demonstrated by the insensitivity of the results to changes in Δt and ϵ_M. A scan in Reynolds number shows that hybrid differencing is more accurate at the higher values, indicating that the first order upwinding is significantly affecting the results [12]. It is plausible that, were we able to use central differencing and a much less contorted mesh, we would select Ciofalo's option. We note in particular that some recent work [13] suggests that the choice of scheme is almost irrelevant, provided the domain is carefully gridded in regions where gradients are high.

3.4 Problems with compressibility

Hybrid differencing was earlier preferred to central in order to ensure convergence of the T calculation, which seems a minimum requirement for any scheme intended later to be applied to the compressible equations. Using hybrid differencing in conjunction with the

compressible option of FLOW3D has not so far proved very fruitful, however, although it must be pointed out that the other schemes typically fail much more violently. The longest run so far made with the 178 × 106 mesh fails after about 100 time-steps.

Just prior to failure, the flow field exhibits a street of vortices that strengthen with distance downstream so that some cores contain supersonic motion. The impression gained is that the outlet boundary condition on pressure is inappropriate. However, even if a better condition could be found, or the mesh be extended further downstream, there remains the difficulty of resolving the now dynamically significant temperature gradients associated with the vortices.

4. Physical Results

4.1 Standard case

We specialise to calculations using the QUICK/Crank-Nicolson option of FLOW3D for space/time differencing. For the standard inlet speed of 50 m/s, giving Re = 470, the results in Section 3 suggest the shedding frequency f is accurate to within a few per cent, although no spatial refinement studies could be performed because of cost. f = 1.4 kHz implies a Strouhal number of 0.25, to be compared with a value 0.20 predicted for a circular obstacle at the same Re [10]. No information is apparently available on the effect of shaping the obstacle, or of placing it near a wall, but it is probable that these effects could account for the discrepancy.

Figure 6 shows the time record of the most accurate run, starting from the standard initial condition. Note that although the velocity field settles down rapidly to regular oscillation, the T-field, as indicated by its maximum value T_{max}, takes longer to reach its asymptotic form. The oscillation in flow variables is caused by the periodic shedding of vortices from edges of the cathode, see Figure 7, which shows a sequence of snapshots (produced using the interactive graphic code G3D [14]) of the temperature and velocity fields at equally spaced times throughout an oscillation. Inspection of e.g. isobars shows the vortices' weakening with distance downstream (Figure 8). Regardless of

sense of rotation, all are regions of lower pressure, but those associated with anti-clockwise motion become predominant far from the cathode. This is physically reasonable in that clockwise vortices are generated close to the channel wall and hence are destroyed preferentially. Or, it can be argued that the wall is a source of positive vorticity that swamps the negative vorticity of the clockwise vortices.

Figure 7 reveals that the sawtooth oscillation of T_{max} is caused by the passage of hot-spots out of the computational domain. The hot-spots form on the colder, trailing edges of vortices, which are regions where flow is decelerated. The greatest temperature is however achieved well downstream of the region containing the heat source, which is unphysical in an incompressible flow. The contrast is only 30°C, sufficiently small that this effect can be ascribed to numerical error. It is interesting to speculate that such hot spots might actually form in the gas laser, where the flow is compressible. The most remarkable effect is that, despite the vortex shedding, the local temperature maximum near the heat source stays almost constant at just below 500°C.

4.2 Reynolds number variation

We first halved the Reynolds number, from 470 down to 235, using the standard initial conditions. The abrupt change in flow speed led to enormous fluctuations in pressure due to the odd-even instability, which although they seem to have little dynamical effect, do increase the cost of run (as many more iterations per timestep are required). Hence we prepared new initial conditions by running with the hybrid/backward differencing option for 600 timesteps at the new inlet speed. A similar procedure was also required when we doubled Re from 470 to 940.

At Re = 235, the flow fields are quite similar in form to those shown in Section 4.1, except that the weaker clockwise eddies are now almost completely absent. As measured by the minimum in the relative pressure p_{min} all eddies turn out to be much less intense, $p_{min} = -25$ instead of -150 Pa. However most other quantities scale close to linearly, e.g. f = 0.66 instead of 1.35 kHz as found in Reference 10. The maximum cross-stream velocity $|v|$ is anomalously smaller, being 42 compared to

97 m/s at the higher Re, so the entrained regions of colder fluid intrude much less into the hot stream. T_{max} varies only from 973 to 978°C during one oscillation.

Doubling the Reynolds number to 940 confirms most of the above trends, e.g. p_{min} = -900 Pa, the oscillations now have a mean f of 2.70 kHz and the cold regions almost completely invade the hot stream. However the clockwise vortices are no more prominent than at Re = 470, and the oscillations have become irregular. The time dependence of T_{max} is particularly remarkable, see Figure 9, changing erratically from 260 to 390°C. Note that T peaks more strongly than at Re = 470 (see Figure 10), suggesting that numerical errors are significantly affecting details of the temperature field.

5. Conclusions

We have obtained converged, time-dependent numerical solutions that model flow in a gas laser, albeit omitting compressibility effects. The runs are very expensive of computer time and obtaining convergence has been a very delicate matter. Nonetheless we believe we have shown that the maximum temperature reached is little affected by the presence of the vortices shed from the cathode. This understanding was more easily obtained thanks to our use of the interactive graphics package G3D [14].

As to the future, some further validation work would seem to be desirable if resources become available, checking whether the computational grid is sufficiently fine near the cathode and the effect of the chosen outlet boundary condition. The least controversial way of performing the latter is to extend the computational domain. Taking accurate account of compressibility effects may be too costly for the immediate future, although some effort could be devoted to analysing the outlet boundary conditions. We remark that the interface to the FLOW3D grid generation package needs drastic improvement before cathodes of other shapes can be easily studied using the code.

Acknowledgements We would like to thank Dr.I.P.Jones and his team at Harwell, especially S.Simcox, for considerable help and advice on the running of FLOW3D, and are very grateful to Dr.F.Briscoe and Dr H.N.Rutt for catalysing this work.

References

[1] Armandillo, E. and Kaye, A.S., (1980) "Modeling of transverse-flow cw CO_2 lasers: theory and experiment," J.Phys. D:Appl.Phys. 11, 321-338.

[2] Burns, A.D. and Wilkes, N.S.,(1987) "A finite difference method for the computation of fluid flows in complex three dimensional goemetries," Harwell Laboratory Report: AERE-R12342.

[3] Burns, A.D., Ingram, D., Jones, I.P., Kightley, J.R., Lo,S. and Wilkes, N.S., (1987) "FLOW3D: The development and application of Release 2," Harwell Laboratory Report: AERE-R12693.

[4] Kaye, G.W.C. and Laby, T.H., (1986) "Tables of physical and chemical constants," Longmans, London.

[5] Van Dyke, M., (1982) "An album of fluid motion," Parabolic Press, Stanford, California.

[6] Jackson, C.P., (1987) "A finite-element study of the onset of vortex shedding in flow past variously shaped bodies," J.Fluid Mech., 182, 23-45.

[7] Jones, I.P., (1988) Private communication.

[8] Batchelor, G.K. (1967) "An Introduction to Fluid Dynamics," Cambridge University Press.

[9] Orszag, S.A. and Kells, L.C., (1980) "Transition to turbulence in plane Poiseuille and plane Couette flow," J.Fluid Mech. 96, 159-205.

[10] Gerrard, J.H., (1978) "The wakes of cylindrical bluff bodies at low Reynolds number," Phil. Trans. Roy. Soc., 288, 351-382.

[11] Ciofalo, M., (1987) Private communication.

[12] Cheng, S.I. and Shubin, G.,(1978) "Computational accuracy and mesh Reynolds number," J.Computational Phys. 28, 315-326.

[13] Boerstoel, J.W., (1988) In "Numerical Methods for Fluid Dynamics III" (K.W.Morton and M.J.Baines eds.), Clarendon Press, Oxford.

[14] Arter, W., (1988) "G3D, a package for interactive graphical analysis of three-dimensional vector and scalar fields," In preparation.

TABLE 1

Summary of runs performed with Re = 470. Timestep Δt is measured in ms, f in kHz, velocity v in m/s and temperature T in °C. ϵ_M is in kg/mm/s, N_{it} is the median number of iterations per time-step: min T denotes the lowest maximum temperature per oscillation, max T the greatest, similarly for $|v|$.

Scheme	$\Delta t \times 60$	$\epsilon_M \times 10^7$	min $\|v\|$	max $\|v\|$	min T	max T	f	N_{it}
Hybrid/	1	10	-	-	501	504	0.68	2
Backward	2	10	-	-	501	504	0.92	6
	1	1	-	-	504	508	1.04	10
HUW/	1	10	53	75	510	515	1.00	5
Backward	1	1	51	72	510	515	1.33	16
QUICK/	1	10	60	80	<506	<510	1.23	6
Backward	1	1	54	77	510	514	1.33	16
QUICK/	1	10	78	100	transient		1.35	6
Crank-Nicolson	2	10	82	100	510	540	1.32	10
	1	1	77	97	500	545	1.37	15

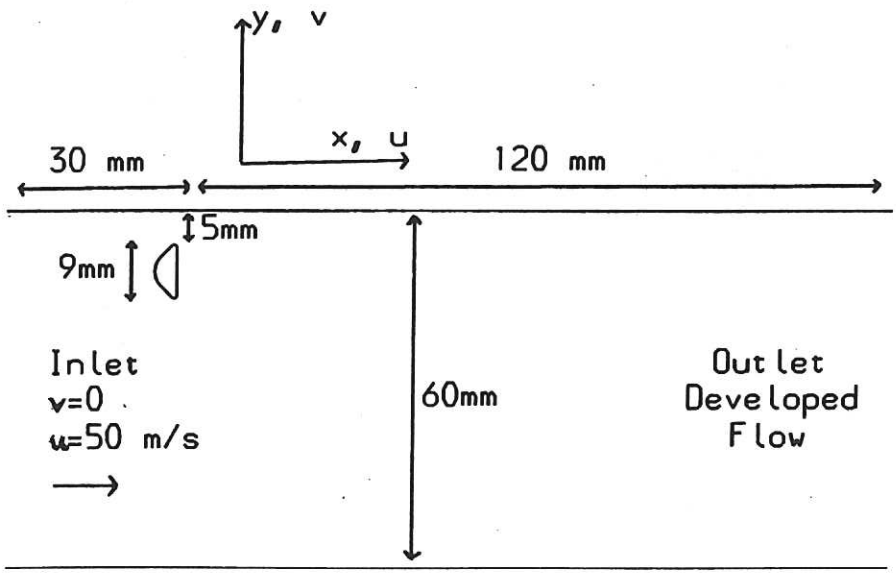

Fig. 1 Geometry of the problem

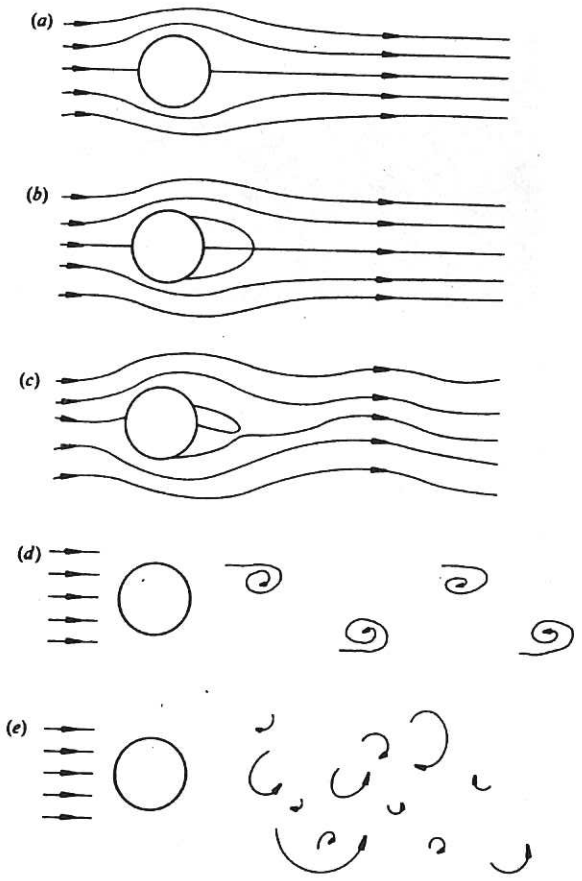

Fig. 2 Schematic dependence of the flow regime on Reynolds number (taken from ref.6).
(a) Very low Re: no separation
(b) $6 \leq Re \leq 50$: separation
(c) $50 \leq Re$: periodic wake
(d) $50 \ll Re$: vortex shedding
(e) Turbulence at very large Re.

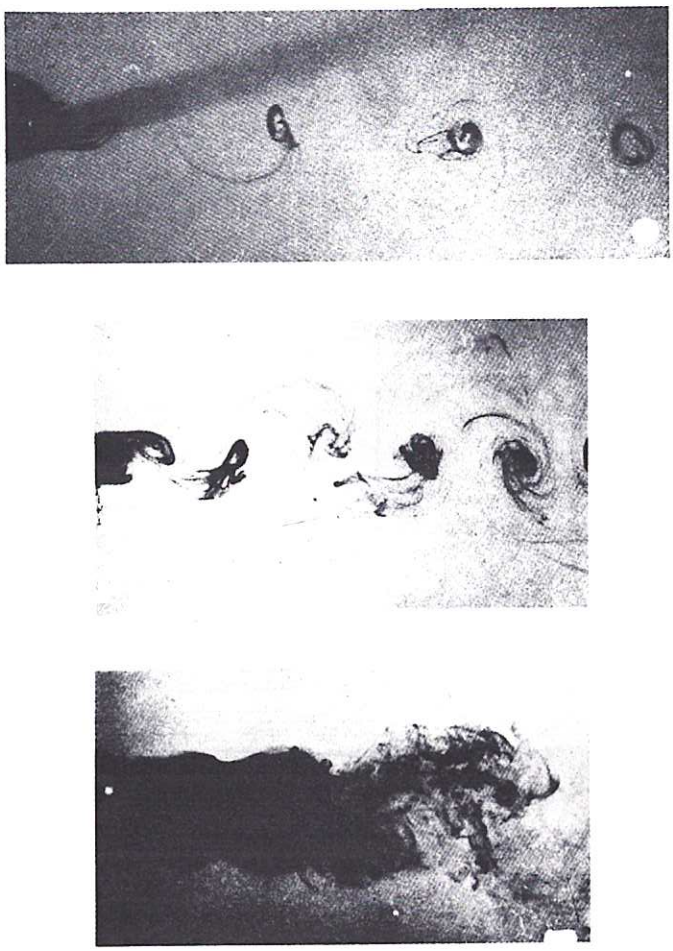

Fig. 3 Wakes of a circular cylinder (taken from ref.10)
(a) $Re=230$ (Fig.30a).
(b) $Re=464$ (Fig. 37).
(c) $Re=1083$ (Fig. 40b).

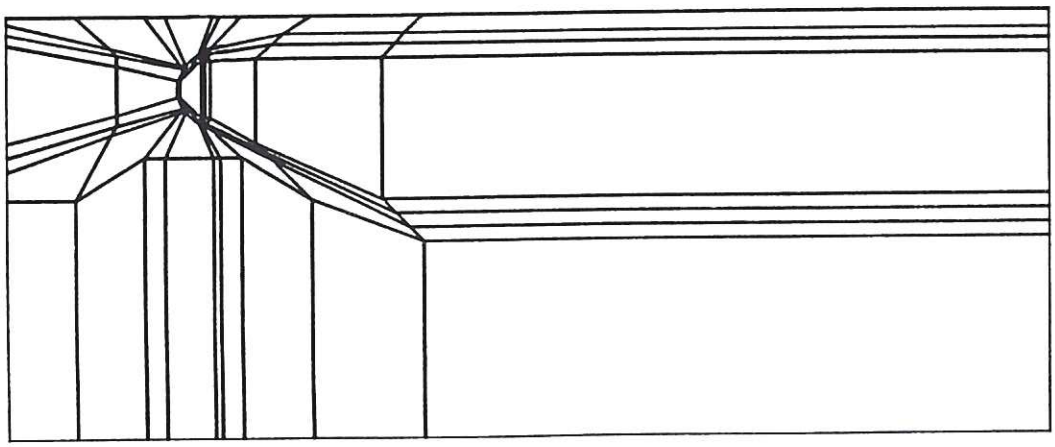

Fig. 4 Constraint lines used in constructing the 178×106 grid. The number of cells between constraint lines, going from left to right in x is: 10, 10, 6, 12, 3, 6, 15, 24, 90 respectively; and from bottom to top in y is: 38, 6, 4, 4, 38, 4, 4, 6 respectively.

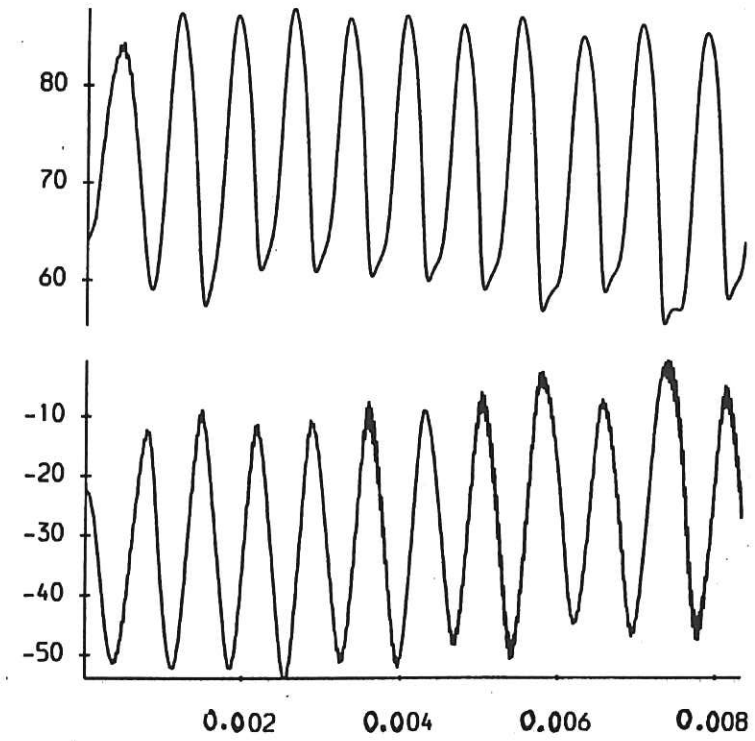

Fig. 5 Plots of u_{mon} (top, in m/s) and p_{mon} (bottom in *Pa*) against time in seconds, for the run at $Re=470$ with $\Delta t=\frac{5}{3}\times10^{-5}$ s and $\epsilon_M=10^{-6}$. u_{mon} and p_{mon} are the values of u and p at the monitoring point just behind the cathode.

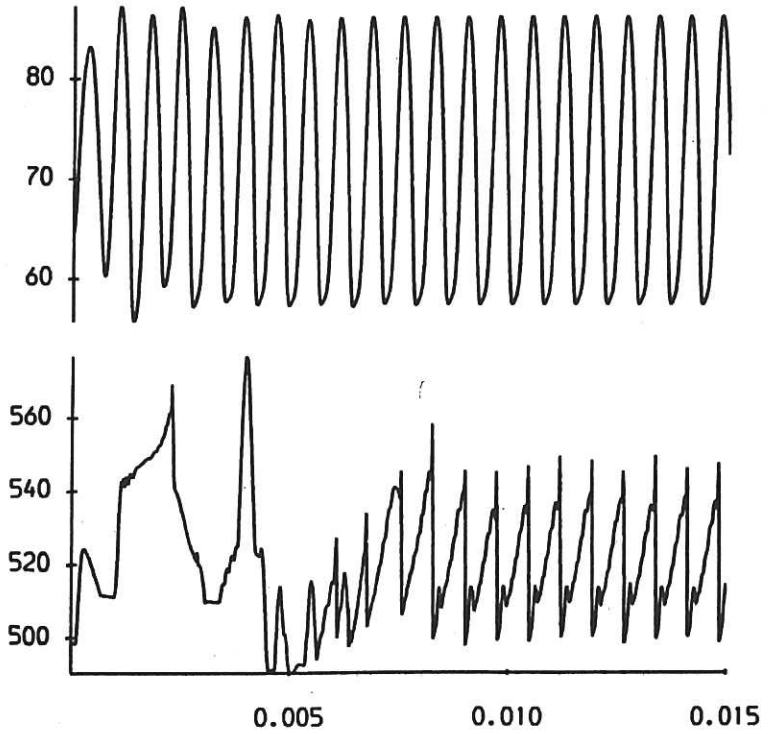

Fig. 6 Plots of u_{mon} (top, in m/s) and T_{max} (bottom, in °C) against time in seconds, for the run at $Re=470$ with $\epsilon_M=10^{-7}$.

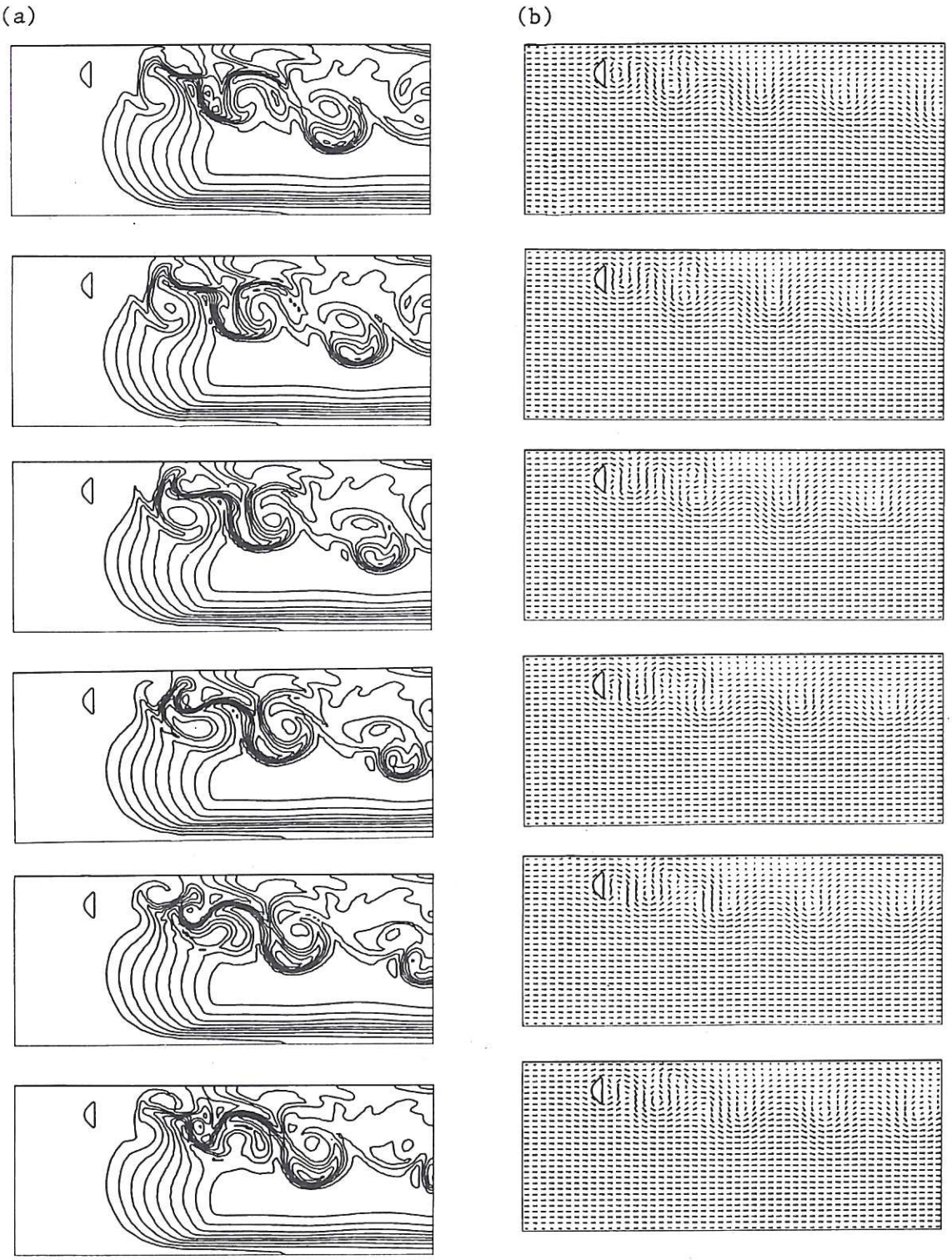

Fig. 7 $Re = 470$ with $\epsilon_M = 10^{-7}$. Plots of fields at timesteps 500 (time = 0.008333 s), 507, . . . , 535, time increasing down the page, showing behaviour throughout one oscillation period.

(a) Isotherms, drawn with contour interval 50°C starting at $T = 50$°C (temperature T increases from the bottom boundary in each plot).

(b) Arrows indicating the direction of the local velocity field and its magnitude by their length made proportional to $(u^2 + v^2)^{0.15}$.

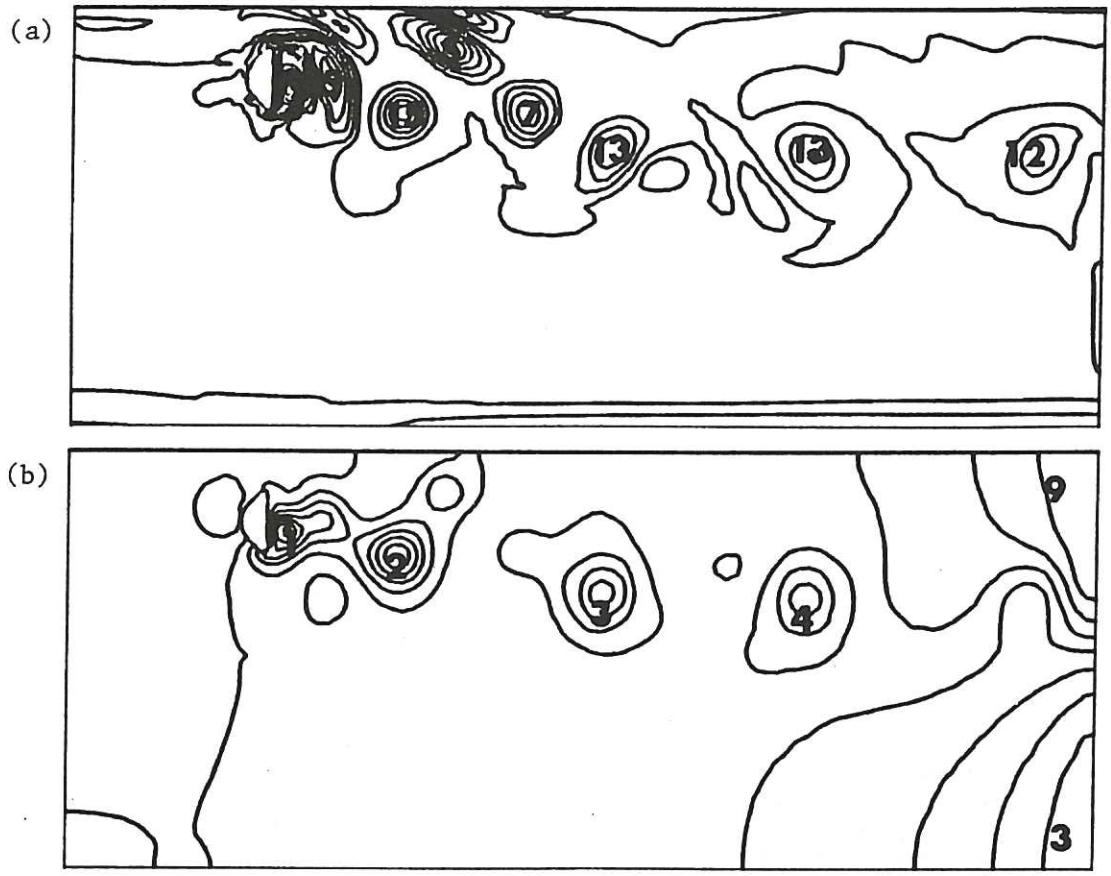

Fig. 8 $Re=470$ with $\epsilon_M=10^{-7}$: fields at timestep 535.
(a) Lines of constant vorticity, drawn at equally spaced values between $-7.38\times10^4 s^{-1}$ (contour 1) and $7.89\times10^4 s^{-1}$ (contour 19).
(b) Isobars, drawn at equally spaced values of relative pressure between -158 Pa (contour 1) and 51.8 Pa (contour 9).

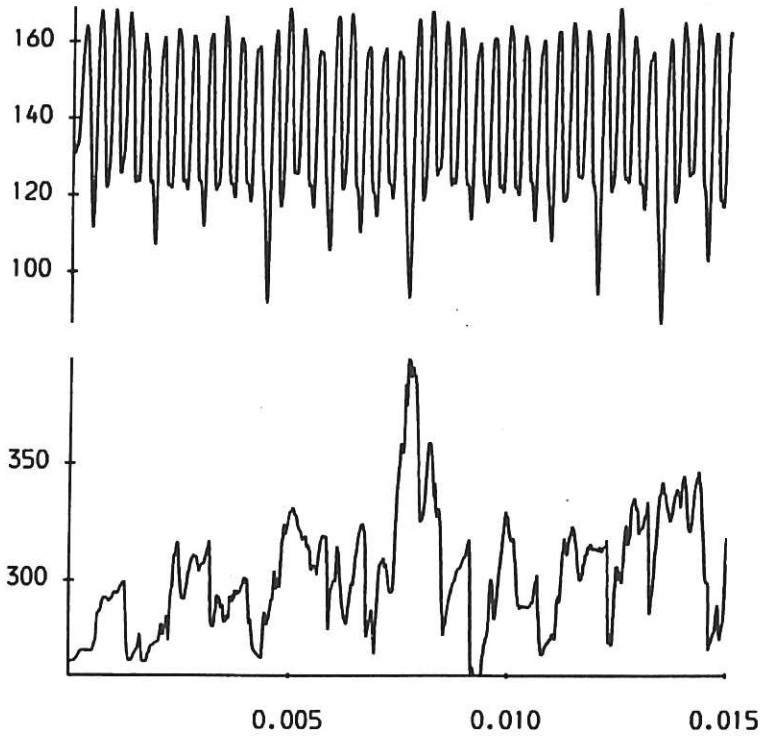

Fig. 9 Plots of u_{mon} (top, in m/s) and T_{max} (bottom, in °C) against time in seconds, for the run at $Re=940$.

(a)

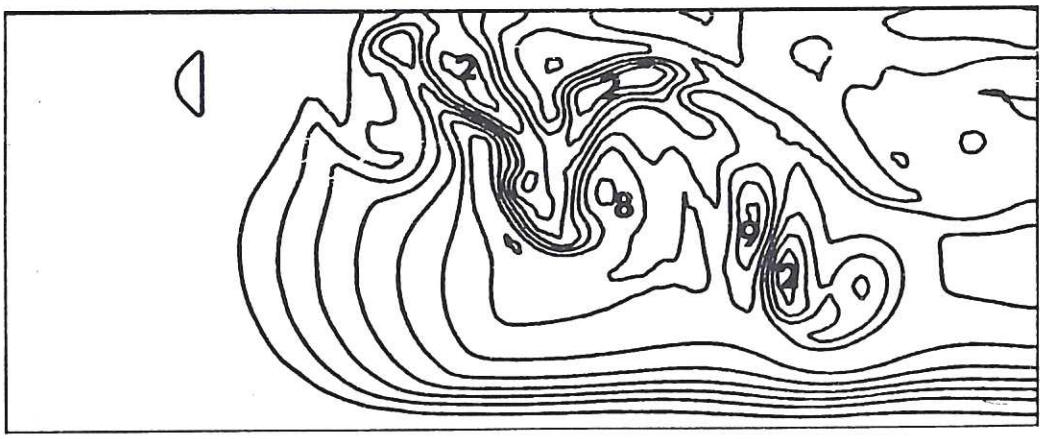

(b)

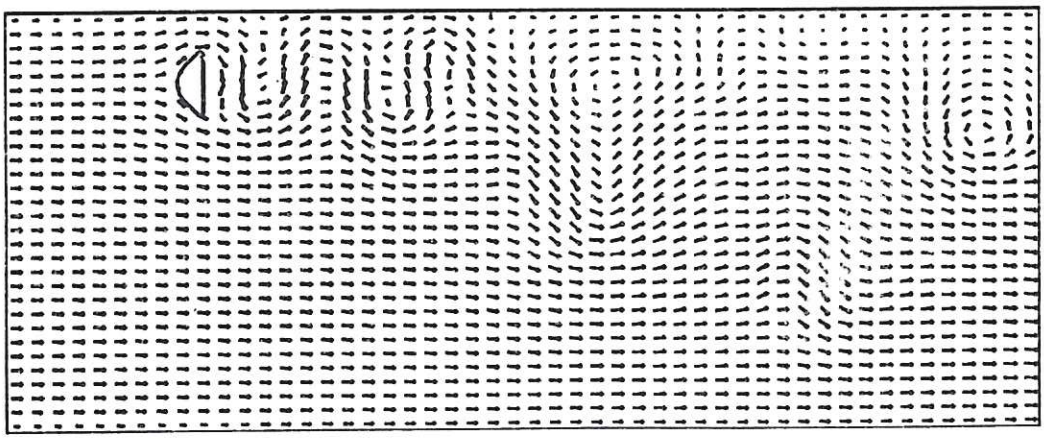

Fig. 10 $Re=940$: fields at timestep 300 (time 0.005 s).

(a) Isotherms, drawn at equally spaced values of T between 41.7°C (contour 1) and 308°C (contour 9).

(b) Arrows indicating the direction of the local velocity field and its magnitude by their length made proportional to $(u^2+v^2)^{0.15}$.

Available from
HER MAJESTY'S STATIONERY OFFICE
49 High Holborn, London, WC1V 6HB
(Personal callers only)
P.O. Box 276, London, SE1 9NH
(Trade orders by post)
13a Castle Street, Edinburgh, EH2 3AR
41 The Hayes, Cardiff, CF1 1JW
Princess Street, Manchester, M60 8AS
Southey House, Wine Street, Bristol, BS1 2BQ
258 Broad Street, Birmingham, B1 2HE
80 Chichester Street, Belfast, BT1 4JY

PRINTED IN ENGLAND